Reverse Engineering and Topology Optimization for Weight-Reduction of a Bell-Crank

Toh Yen Pang * and **Mohammad Fard**

School of Engineering, RMIT University, Bundoora Campus East, Bundoora, VIC 3083, Australia; mohammad.fard@rmit.edu.au

* Correspondence: tohyen.pang@rmit.edu.au; Tel.: +61-3-9925-6128

Abstract: This paper describes a new design method that was developed to achieve an optimal design method for weight reduction of a bell crank, sourced from a Louis Christen Road Racing F1 Sidecar. The method involved reverse engineering to produce a 3D model of the mechanical part. The 3D bell crank model was converted to a finite element (FE) model to characterize the eigenvalues of vibration and responses to excitation using the Lanczos iteration method in Abaqus software. The bell crank part was also tested using a laser vibrometer to capture its natural frequencies and corresponding vibration mode shapes. The test results were used to validate the FE model, which was then analysed through a topology optimization process. The objective function was the weight and the optimization constraints were the stiffness and the strain energy of the structure. The optimized design was converted back to a 3D model and then fabricated to produce a physical prototype for design verification and validation by means of FE analysis and laboratory experiments and then compared with the original part. Results indicated that weight reduction was achieved while also increasing the natural frequency by 2%, reducing the maximum principal strain and maximum von Mises stress by 4% and 16.5%, respectively, for the optimized design when compared with the original design. The results showed that the proposed method is applicable and effective in topology optimization to obtain a lightweight (~3% weight saving) and structurally strong design.

Keywords: bell crank; topology optimization; natural frequency; reverse engineering; vibrometer; design; Abaqus

1. Introduction

A bell crank is a mechanical component that is primarily responsible for translating the motion of links through an angle. It acts as a link between a spring and a damper component at one end, and a pushrod/pull rod at the opposing end. The most common limitation associated with vehicle suspension in racing vehicles is the inability to mount the spring/damper mechanism vertically, compared with most ordinary cars. As a result, bell cranks are incorporated into the design of racing vehicles to translate the vertical motion of the wheel into horizontal motion to allow the suspension to be mounted transversely or longitudinally [1].

However, in racing vehicles, there are limitations on bell cranks that relate to their weight. When there is a limit in engine power capacity, a reduction in vehicle mass will improve the performance aspect of a racing vehicle known as a power-to-weight ratio. Hence, engineers are constantly trying to improve the performance of bell crank by reducing its weight, while maintaining its structural integrity. To achieve that, engineers have been using the structural topology optimization method to find an optimal material distribution in a structural design domain considering an objective function in presence of constraints [2–5].

However, only a limited number of studies in the literature examined topology optimization of bell cranks [4,6,7]. Fornace [6] used a topology optimization method to assess weight reduction of bell cranks for a Formula Society of Automotive Engineers (SAE) vehicle. The author considered reducing the mass of the rear bell crank component by at least 10% while maintaining the yield strength of the previous design. The author utilized destructive testing on three specimens under static loads of 445 N to validate their new design. Choudhury et al. [4] used a 'Fully Stressed Design' optimization procedure to achieve the mass and stress optimization of bell crank of Formula SAE vehicle from SRM University Chennai in India. The procedure allowed them to investigate and analyze the structural stress distribution of the bell crank in real-time conditions during the damping process and the spring actuation. The authors managed to produce an optimized computer aided design (CAD) bell crank model with a 22% and 20% of overall weight and stress reduction, respectively.

When reducing the mass (or volume) of a mechanical component such as bell cranks, engineers face challenges to maintain structural integrity. The structural integrity relevant to a mechanical component is its overall stiffness. An element that directly correlates with component stiffness is its natural frequency. The natural frequency of a certain vibration mode can be controlled in order to reduce the displacement or deformation of a particular point in the structure [8,9]. Thompson et al. [10] found that chassis stiffness is directly related to its flexibility when the stiffness of the chassis increases, the twist vibration decreases and the overall vehicle handling is improved by allowing the suspension components to control a larger percentage of the vehicle's kinematics.

No studies in the literature have utilized a non-destructive mode shape analysis to investigate the dynamic response of the bell crank. The benefit of using mode shape analysis is that it allows engineers to determine the dynamic stiffness of a structure. By changing the stiffness of the structure, engineers could minimize the amount of vibration, which is produced by the relative motion or deformation of the structure under applied loads [11]. In the case of the bell crank, a small relative motion in the suspension system will provide undesirable feedback to the operator in either lateral, longitudinal or cyclic loadings [12].

The purpose of this study is to propose a methodology that incorporates a reverse engineering technique and physical testing for accurately and efficiently assessing topology optimization problems.

2. Theory of Weight Reduction and Stiffness Matrices

2.1. Modelling Approach

In a static structural analysis, for an arbitrary structure that is subjected to external forces and under the prescribed boundary conditions, the FE matrix equation can be expressed as [13–15]:

$$[F] = [K]\{u\} \tag{1}$$

where $[F]$ the force vector, $[K]$ the stiffness matrix, and $\{u\}$ the displacement vector [16].

According to Guyan [13], the vector $\{u\}$ can be partition into boundary degrees of freedom (DOF) and internal DOF, and they are denoted with subscript of b and i, respectively. Equation (1) is fully general and is applicable for two-dimensional and three-dimensional problems, with appropriate boundary conditions. The entire system can be partitioned to [14]:

$$\begin{Bmatrix} F_i \\ F_b \end{Bmatrix} = \begin{bmatrix} k_{ii} & k_{ib} \\ k_{bi} & k_{bb} \end{bmatrix} \begin{Bmatrix} u_i \\ u_b \end{Bmatrix} \tag{2}$$

Once the global stiffness matrix $[K]$ is assembled, the unknown nodal displacement, $\{u_i\}$ and unknown reaction forces, $[F_b]$ can be obtained by solving Equation (2). From the first line of equation, we first solve for $\{u_i\}$, i.e., $u_i = k_{ii}^{-1}(F_i - k_{ib}u_b)$; subsequently, substitute u_i into the second line of equations, and thus F_b can be solved as $F_b = k_{bi}u_i + k_{bb}u_b$.

2.2. Topology Optimization: Structural Compliance

Once the nodal displacements and reaction forces are calculated from Equation (2), the topology optimization is to determine the optimal subset Ω^* of material distribution of a given design domain, Ω. The generalized formulation [16,17] for the compliance of the design domain is given as:

$$C^{\Omega}(x_e) = F_i^T(x_e)\, u_i(x_e) - F_b^T(x_e)\, u_b \tag{3}$$

where x_e is the vector of design variables.

Assuming a structure that is subjected to the prescribed external loads and under appropriate supports, the design domain is meshed with N finite elements. To achieve a reduction in mass, the topology optimization statement is expressed as [5,16,18–20]:

$$\text{Find}: \rho = \{\rho_1,\, \rho_2,\, \cdots,\, \rho_N\}$$

$$\text{Minimize}: [F]_\rho^T\{u_\rho\}, \tag{4}$$

$$\left.\begin{array}{l}\text{Subject to}: \int_\Omega \rho(x_e)d\Omega = Vol(\Omega^*) \le V \\ \qquad\qquad : 0 < \rho_{\min} \le \rho(x_e) \le 1\end{array}\right\} \tag{5}$$

where V is the total initial volume before optimization, and $\rho_{\min}$ is the lower bound of artificial material density, $\rho(x_e)$ of each element in the design domain, which can be determined:

$$(x_e) = \left\{\begin{array}{l} 1 \text{ if solid, } x_e \in \Omega* \\ 0 \text{ if void, } x_e \notin \Omega* \end{array}\right. \tag{6}$$

The displacement vector u_ρ, which is the function ρ in Equation (4) can be obtained by solving:

$$[K(\rho(x_e))]\{u\} = [f] \tag{7}$$

where $[K]$ is a structural global stiffness matrix and is obtained by the assemblage of element stiffness matrix over the design domain. For a given isotropic material, the stiffness matrix of each element, which depends on its artificial material density $\rho(x_e)$ is given by the following Young's modulus:

$$E(x_e) = \rho(x_e)\overline{E} \tag{8}$$

where $\overline{E}$ is Young's modulus for the given isotropic material, which assumed to be the same for all elements. When in equilibrium state, the energy bilinear form (i.e., the internal virtual work done by the elastic body, within a given design domain Ω) can be expressed as [18,19]:

$$\delta W(v,\, w) = \int_\Omega E(x_e)\varepsilon_{ij}(v)\varepsilon_{kl}(w)dV \tag{9}$$

where $E(x_e)$ the optimal stiffness tensor that attain the isotropic material properties, V is the given total material volume, v the internal work at equilibrium state, w an arbitrary virtual displacement, and with linearized strains $\varepsilon_{ij}(v) = \frac{1}{2}\left(\frac{\partial u_i}{\partial x_j} + \frac{\partial u_j}{\partial x_i}\right)$ and linearized load as $l(v) = \int_\Omega f\delta u d\Omega + \int_{\Gamma_T} t\delta u dS$.

The first integral extends over the volume of the body and the second integral extends the surface of the body.

We know strain energy is stored within an elastic body when the body deformed under the external forces. The objective function in Equation (4) is to achieve the optimal design via minimize the structural strain energy, which can be expressed as:

Minimize: $C = \{u\}^T[K]u$

Subject to: $[K(\rho(x_e))]\{u\} = [f]$

2.3. Vibration and Eigenvalue Problems

The eigenvalues of vibration and responses to an excitation mechanism play an important role in the design process. Likewise, the efficiency and accuracy of the FE analysis that solves the eigenvalue problem plays a crucial role in the success of present topology optimization of continuum structures [21]. Consider the linearized equation of motion for a vibration excitation in a discrete undamped structure [15,22,23], in our case the bell crank, can be expressed in the form:

$$M\ddot{q} + Kq = F \tag{10}$$

with M and K the global mass and stiffness matrices of the structure, F is the force vector, and q is the vector of unknown displacement DOF.

The solution of Equation (10) results in an eigenvalue problem, with ω are the eigenvalues and ϕ^N the associated eigenvectors, which can be expressed as [23]:

$$\left(-\omega^2 M^{MN} + K^{MN}\right)\phi^N = 0 \tag{11}$$

where M^{MN} is the mass matrix, K^{MN} is the stiffness matrix, and M and N are the DOFs. The eigenvalues of Equation (11) are usually solved using the Lanczos or subspace iteration method.

3. Materials and Methods

3.1. Overview of the Process

The overall design optimization process of the proposed study is summarized in Figure 1. The process started with a physical bell crank, which went through non-destructive experimental tests and a reverse engineering process to create an equivalent finite element (FE) model. The experimental data were used to verify the FE model. The optimization was based on the generalized process of finding a solution to the objective functions, which were either to be maximized or minimized material distributions within a design domain [24]. The design domain was subjected to constraints (e.g., material layout within a given design space (volume constraint) or maximum stress values) to be satisfied.
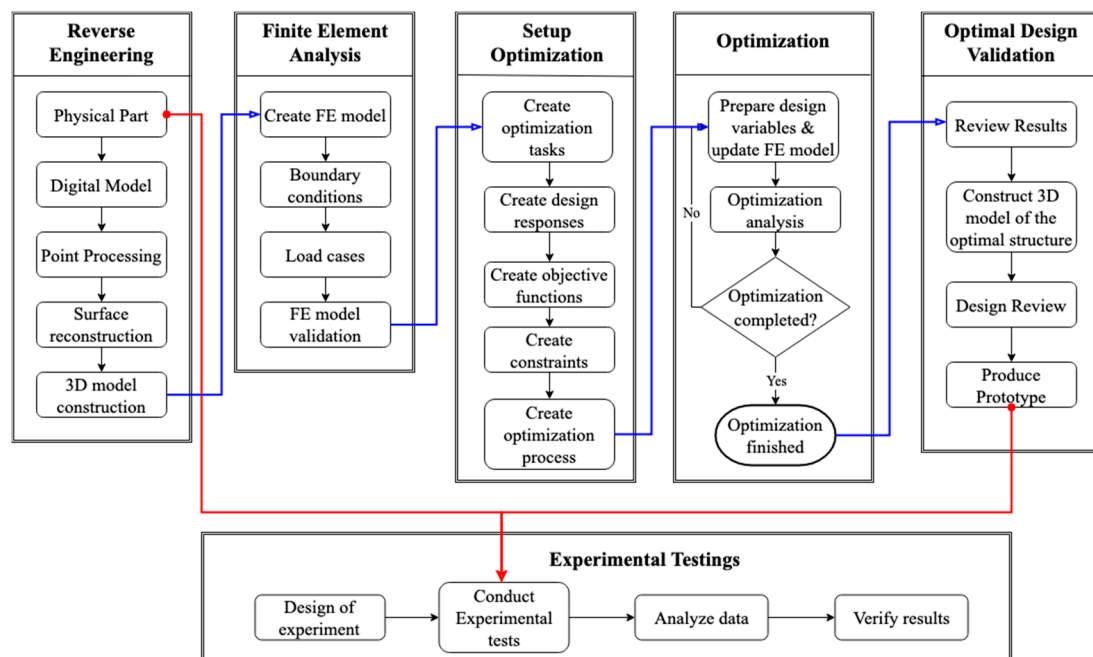

Figure 1. Flow chart depicting major stages of design optimization approach.

3.2. Physical Part of Reverse Engineering

The detail drawings and three-dimensional (3D) model for the bell crank were not available. Therefore, a reverse engineering technique known as 3D scanning was used to create a 3D model of the bell crank.

A bell cranks sourced from a Road Racing Sidecar and produced by Louis Christen Racing (LCR) in 1994, was used for the present study. The bell crank is made of anodized aluminum (Figure 2a) and its surface luster is relatively high, which resulted in a 'noisy' scan. Hence, the shiny surface required a coating that minimized the unwanted scanning noise. A product named *'PlastiDip'* in solid Matte White was used to coat the bell crank to achieve a matte finish surface. The coated bell crank was then placed on the rotating table and scan images were captured with FlexScan (Figure 2b). All scanned images were merged to create the shape of a 3D part model. In various locations, FlexScan was unable to duplicate the exact specifications and dimensions of the bell crank. Hence, a clean-up of the 3D model was necessary (highlighted in yellow (Figure 2c)). The surface of the material was cleaned using a '*defeature tool*' within 'Geomagic'. Holes were filled using the '*fill-up tool*'. Before the model was converted into an '*igs*' format, a '*mesh doctor*' tool was used to remove non-manifold edges, self-intersections, highly creased edges, spikes and small components. Various modifications of the 3D model were performed in the CATIA (V5R21) computer-aided design (CAD) program to assure the 3D model replicated the accurate dimensions and features of the actual bell crank. Figure 2d shows the revised and final 3D model that was then used for the validation and optimization tasks.
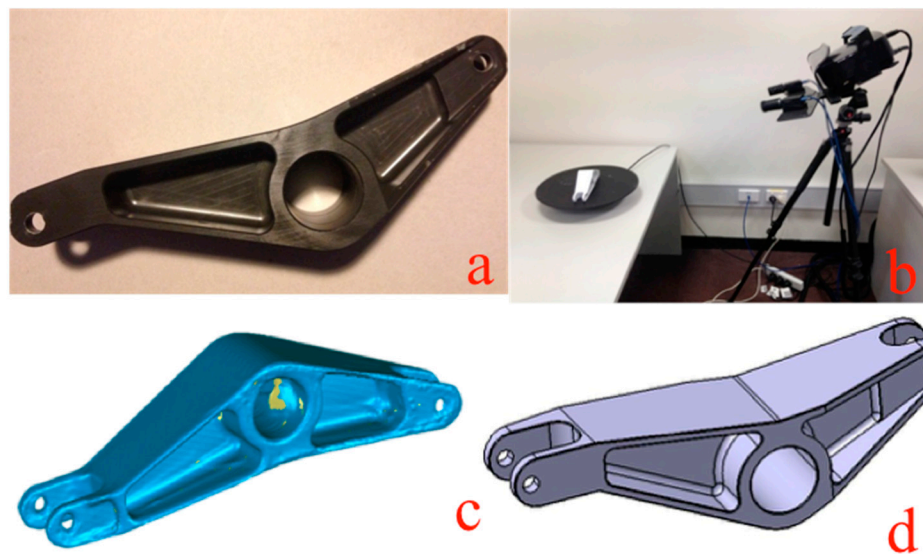

Figure 2. Bell crank scanning process: (**a**) Actual bell crank; (**b**) 3D scanning of the bell crank with FlexScan; (**c**) initial scanned 3D model; (**d**) final 3D model.

3.3. Experiment Method

Since only one bell crank part was available, a non-destructive method was adopted. The bell crank was tested using a laser vibrometer (PSV-400 Scanner, Polytec Inc., Irvine, CA, USA, coupled with the Polytec scanning program), which uses non-contact laser measurement [25]. The schematic diagram of the experimental equipment used for vibration testing is shown in Figure 3a. The bell crank was suspended in the air with strings, which has minimal damping characteristics, through the holes. The experiment's approach was aimed at extracting the modes of the frequency of the bell crank through applied sinusoidal vibration at five different points. The bell crank was excited by a modal shaker (model 2007E, miniature electrodynamic shaker, Cincinnati, OH, USA) as a sinusoidal force at predefined locations, indicated in Figure 3b. The tests were repeated five times at each location, so average eigenvalues for each location could be extracted. A mesh grid (x = 50, y = 20) was created

over the top face of the bell crank, as this sizing of the grid gave the greatest coverage for the analysis (Figure 3c). Across the top face of the bell crank, the laser pointer recorded each separate point for a response. The laser vibrometer captures the natural frequencies and the corresponding vibration mode shapes of the bell crank in the required frequency band.
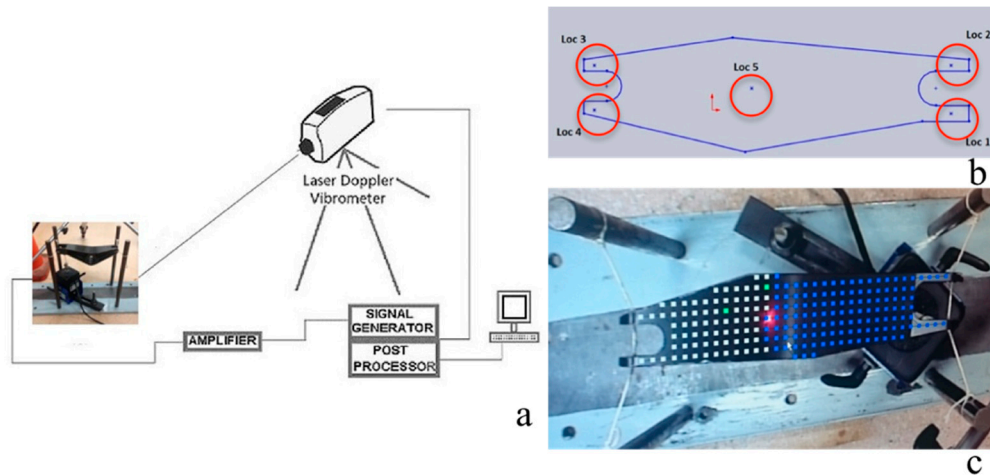
Figure 3. (**a**) Vibrometer test setup, (**b**) Locations for modal shaker attachment, (**c**) Scanning grid on top face of bell crank.

3.4. Bell Crank Model Validation

The 3D bell crank model was imported into the simulation program (Abaqus v6.14 [26]) for running a natural frequency analysis. Model geometry, material properties, element type, boundary conditions, step-to-request frequency modes, and a detailed description of the modelling are outlined in the following sub-sections.

3.4.1. Finite Element Mesh and Material Properties

The element size of the bell crank was set at 3 mm, and the 10-node quadratic tetrahedron element was chosen as the element type.

Figure 4 shows the meshed bell crank, which contains 20,827 elements and 35,803 nodes to the solid section. The mechanical properties of AW-6082-T6 aluminum alloy were assigned to the bell crank model [27,28]. The material properties used for the bell crank are as follows: Yield strength, f_y = 310 MPa, density, $\rho = 2.7 \times 10^{-9}$ kg/mm^3, Young's Modulus, E = 70 GPa and Poisson's ratio, $\nu = 0.33$.

Figure 4. Tetra-meshed of the 3D bell crank FE model.

3.4.2. Boundary Conditions

Boundary conditions were set up to replicate the best testing scenario previously conducted using a laser vibrometer. The bell crank was suspended by the string to avoid any external forces impeding

the modal shaker; hence, the corresponding boundary conditions were imposed on the FE model. The two holes at either end of the FE model were restricted in both linear and rotational X, Y and Z directions. The eigenvalues of vibration and responses to excitation for the FE bell crank was determine using Equation (11) through the Lanczos iteration method in Abaqus software. The results obtained from the vibrometer testing were used for validation of the eigenvalue or natural frequency of the 3D bell crank FE model.

4. Bell Crank Optimization

4.1. Optimization Problem Statement

The optimization algorithms are based on published work [18,19,29]. Topology optimization for a continuum structure can be regarded as a material distribution problem, where the target is to find an optimized material distribution within the design domain, for the minimum compliance (or maximum global stiffness) according to Equation (3). Since $Stiffness \propto \frac{1}{Compliance}$, minimizing the compliance will maximize the stiffness.

In this study, the bell crank was discretized into finite elements and the Abaqus Topology Optimization Module (ATOM) was used to search for a minimum compliance design to minimize strain energy or compliance, based on the boundary conditions and forces being applied to the bell crank. The bell crank was discretized into finite elements. Assuming a constant E_e for each element, and using Equations (4) to (7), the discrete form can be expressed as:

$$\text{Minimize}: \ C = \{F\}^T\{u\} \text{Subject to } [K \cdot E(x_e)]\{u\} = \{F\}$$

where $E(x_e) \in E_{ad}$, $K = \sum_{e=1}^{N} K_e(E(x_e))$, summing $e = 1, \dots, N$ elements. The objective function for this study was to minimize the overall displacements $\{u\}$, and a global measure of displacements is the strain energy, thereby minimizing the strain energy according to Equation (9).

$\{F\}^T$ represents the forces applied, $[K]$ is the global stiffness matrix, which depends on the stiffness of the individual elements E_e, whereas E_{ad} is a set of admissible stiffness tensors for design problems. The entire design optimization process is summarized in Figure 5.
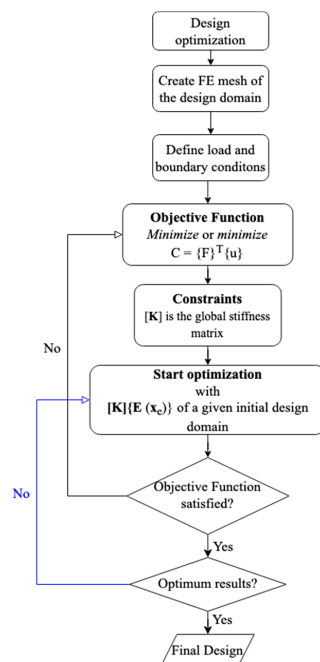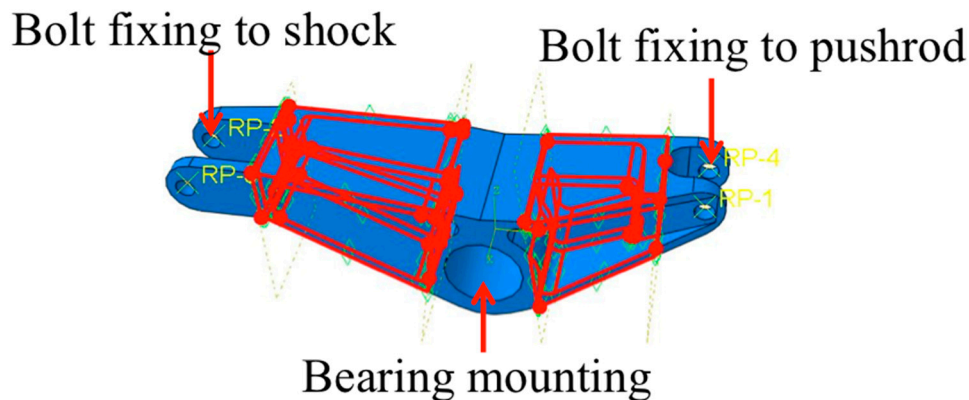

Figure 5. The design optimization process.

Figure 6. Design domains topology optimization (highlighted in red).

4.2. Topology Optimization of the Bell Crank

For the topology optimization analysis, only two design domains of the bell crank were considered to find an optimized material distribution. The regions were highlighted in red in Figure 6. The regions, which cannot be affected by the topology optimization, were located at the center bearing and the bolt holes on either end of the bell crank.

4.3. Boundary Conditions

During the optimization process, the bell crank model was subjected to two different boundary conditions. The first was applied to restrain all degrees of freedom at the center bearing hole. The second consists of point loads at four different locations. The loading forces were obtained from the Eibach Motorsport Catalogue 2014 [30], based on the 100-60-0080 spring, which is featured on the sidecar. A force value of 5299 N was provided as the block height of the spring and, therefore, will be considered as the worst-case loading scenario. Due to the pushrod and suspension orientations within the vehicle, these forces were divided into horizontal and vertical components. A horizontal force of 460 N and a vertical force of 2609 N were applied as a concentrated force at each reference point location indicated in Figure 7.
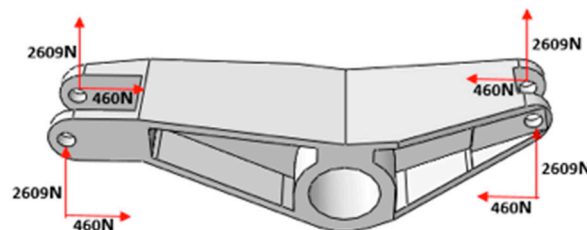

Figure 7. Applied boundary conditions for topology optimization.

5. Results and Discussion

5.1. Experimental Testing Natural Frequency

Values of natural frequency for the bell crank at the five tested locations are presented in Table 1. Note that an average natural frequency of 5046.75 Hz was obtained for all tested locations.

The value for the stiffness of the bell crank was 417.81 MN/m, which was solved by derivation of the natural frequency equation. The results obtained in the vibrometer testing were then used for validation of the 3D bell crank model before the topology optimization process.

Laser vibrometer measuring has high accuracy without causing any damage to the test object. However, displacements of a freely suspended test object during the acquisition process is a common source of minor error in the method [25]. However, in the measurement setup for this study, the bell

crank was constrained by strings through the two side holes to ensure stability and to avoid any large displacement of the laser focal point during the data acquisition process. Hence, the properly constrained bell crank has enhanced the repeatability of the test results.

Table 1. Vibrometer Test Results.

Location	Mean Peak Frequency (Hz)	Standard Deviation
1	5061.25	1.30
2	5036.25	0.98
3	5045.00	1.15
4	5053.75	1.04
5	5037.50	0.64

5.2. Finite Element Model Validation of Natural Frequency

The accuracy of the created FE bell crank model was investigated through a proper process of validation to minimize any modelling errors, including the element and discretization errors (meshing), and the input errors from boundary and loading conditions [31]. Table 2 represents the results obtained from the natural frequency analysis of the FE bell crank model. The mode shapes from the FE model were analyzed to find the one that best represented a sinusoidal wave as observed in the physical test. It was found that, during the vibrometer testing, the first natural frequency was found in the fourth mode shape.

Table 2. Finite element bell crank modal analysis results.

Mode	Frequency (Hz)
1	1714.5
2	2560.7
3	2864.2
4	5285.7

A similar mode shape result was found in the FE bell crank model (Figure 8), which displayed a sinusoidal motion at the fourth mode with a resonant frequency of 5285.7 Hz.
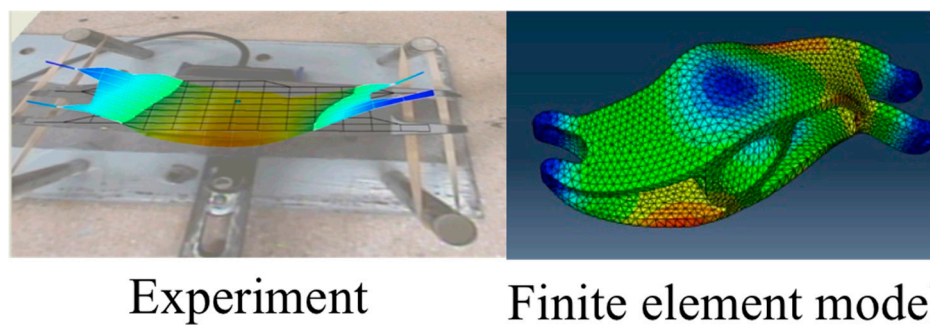

Figure 8. Fourth mode shapes of the physical bell crank and finite element model.

When analyzing both experimental and FE results, the difference in the natural frequency at the fourth mode of each case is below 5%; hence, the FE bell crank model achieved a satisfactory validation against the vibrometer experimental test. The validated FE bell crank model was then used for further topology optimization analysis.

5.3. Topology Optimization

A strain energy design response and a volume constraint were assigned in the optimization module. To improve the stiffness of the bell crank, the strain energy design response was assigned as

the "minimizing strain energy". The stiffness of the structure was determined by its displacement corresponding to the assigned boundary conditions [32]. The volume constraint was assigned as it directly related to the overall mass of the bell crank model. In the analysis, a range of volume constraints, i.e., 95%, 90%, 85%, 80% and 75% of the original volume, was assigned to the FE model to achieve the optimal design.

Figure 9 shows the progressive removal and grouping of elements from the topology optimization analysis. At the volume constraint of 95%, the top surface and the two opposing arm locations of the bell crank (indicated by green contour) demonstrated a potential for element removal. Once the volume constraint was reduced to 90%, a significant material reduction was observed on the left arm region. From the 85% to 80% volume constraint results, significant reductions of material on both arm regions, as well as on the edges at the top of the bell crank, were achieved. The 75% volume constraint in the topology optimization featured the highest amount of material removal.
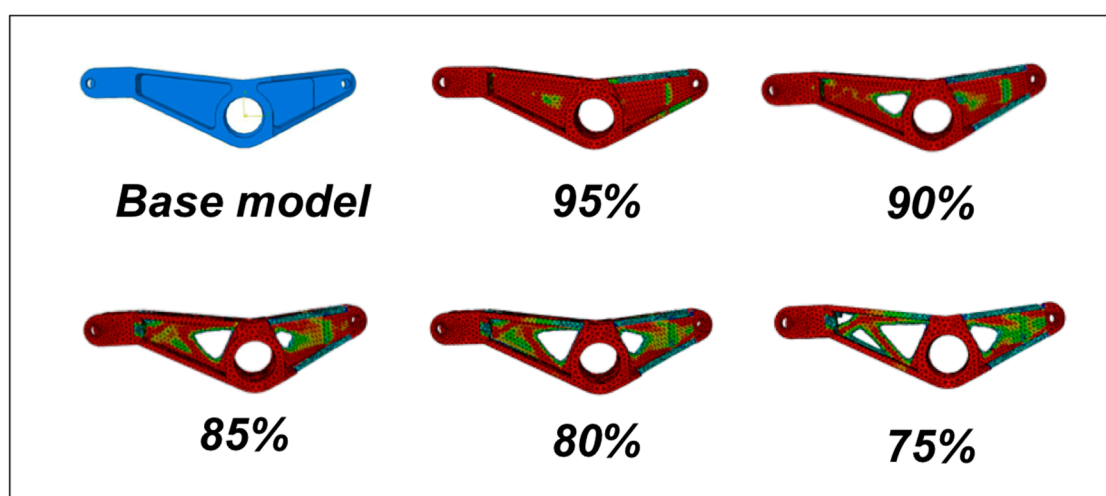

Figure 9. Topology optimization results with associated volume constraints, side view.

5.4. Design Validation

5.4.1. Geometry Interpretation and FEA

Topology optimization often produces complex contours in the geometry, which may be difficult for manufacturing and/or machining [8,33]. The results obtained from the iteration process of the topology optimization were used as guide geometries to determine where material should be withdrawn from the design domain. The guide geometries were interpreted toward the creation of optimal designs with suitable shapes and features for both machining and practical purposes. The guide geometries were exported from Abaqus into CATIA (V5R21), where their shapes and features were traced in the CAD environment. The optimized CAD design for the volume constraint models, i.e., 95%, 90%, 85%, 80%, and 75%, were then created.

To overcome unrealistic contour issues, the geometry was simplified to produce a practical optimized part. Sharp edges obtained through the topology optimization iterations were rounded with fillets, with a minimum radius of 3 mm for ease of machining. Profiles were smoothed out, due to the checkerboard contours resulting from the removal of elements. An example of the CAD design for the 80% volume constraint model is shown in Figure 10.

Re-analysis was carried out to assess the efficiency and structural integrity of the optimized bell crank design. The same 'static-general' and frequency-finite element tests were conducted, as examined on the original model, with identical set-ups of boundary and loading conditions. The maximum von Mises, stiffness, mass and maximum principal strain for the optimal design produced in the topology optimization with different volume constraints are shown in Figure 11.
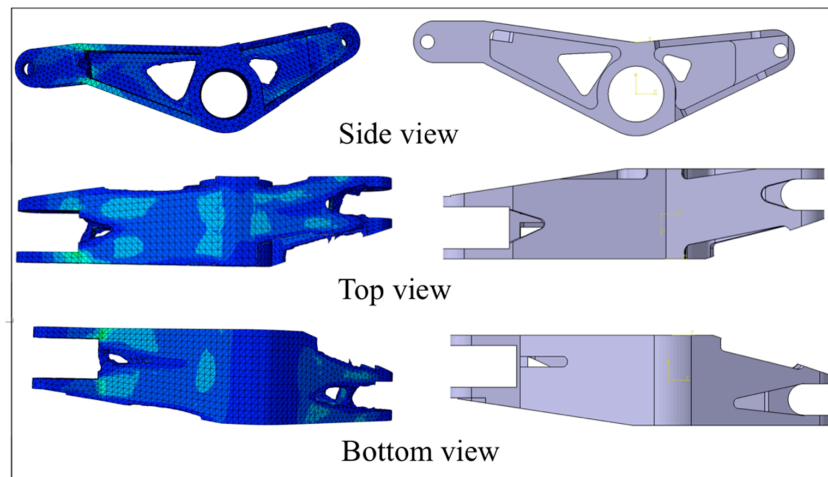
Figure 10. Revised CAD model for the 80% volume constraint. (**Left**) Optimization model, (**Right**) the CAD design free of irregular and complex shapes.
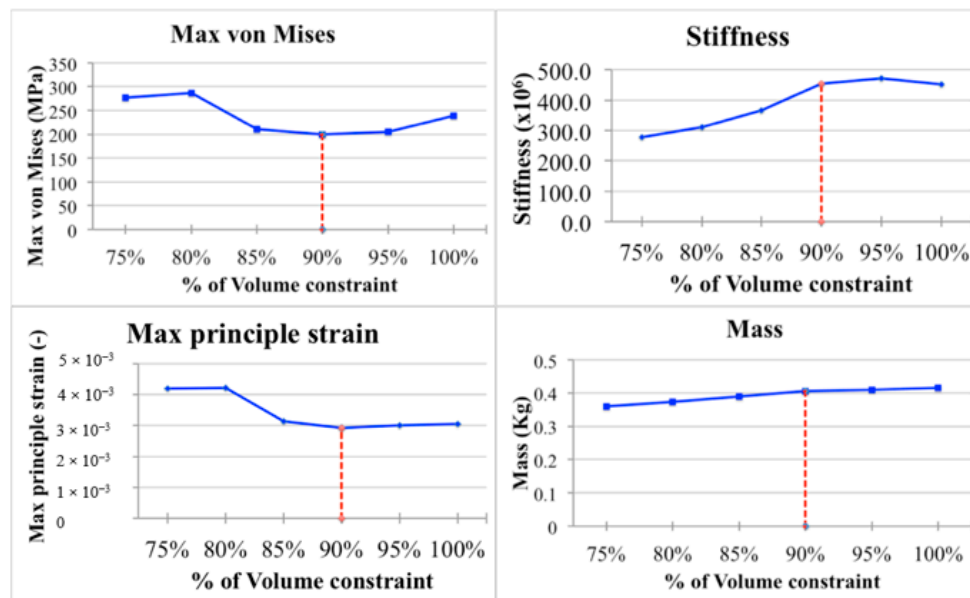

Figure 11. Summary of the structural integrity of the optimized bell crank CAD design.

The optimization results show that the 90% volume constraint model produced higher values of stiffness, with a corresponding natural frequency of 5334 Hz. It also featured a 16.5% reduction in maximum von Mises stress value, a 4.3% reduction in maximum principal strains, and a decrease in weight by 10 g from the original bell crank. The finite element result indicated that the highest stress concentration in the optimized model was 199.76 MPa. Based on the part that was machined out of Al6082-T6, the corresponding yield stress value was 310 MPa, which indicated a safety factor of 1.55 for the optimized bell crank. Hence, through the optimization iteration processes, the 90% volume constraint model was considered as the optimal design.

It is worth noting that the main technical challenges of converting the optimized FE analysis topological results in CAD design for further analysis and manufacturing. As highlighted previously by other investigators [29,33] and the current study, the initial topology optimization results still required manual process to eliminate holes, shape, irregular and complex edges, for example, see Figure 10. The topology optimization results were manually reconstructed to smoothen the shape and complex edges and to fill the missing pores to improve its manufacturability to the final design before the fabrication commencing.

5.4.2. Bell Crank Prototype Fabrication

After validating the FEA model, the prototype of the bell crank was fabricated for the next stage of physical testing and validation. A MU500VII-L 5-Axis Vertical Machining Station (Okuma, Charlotte, NC, USA) was used to machine the prototype. Due to cost limitations and the availability of the material, the optimized bell crank was machined out of Al6061 aluminum. The mechanical properties of Al6082-T6 and Al6061 are very similar, and the density, modulus of elasticity and Poisson's ratio all remain the same. The differences were in reductions in yield strength from 260 N/mm^2 to 240 N/mm^2 and tensile strength from 310 N/mm^2 to 260 N/mm^2. The changes in yield and tensile strength did not alter the result of the eigenvalue simulation and, therefore, did not alter the validation result from the laser vibrometer testing. The machined version of the optimized bell crank is illustrated in Figure 12.
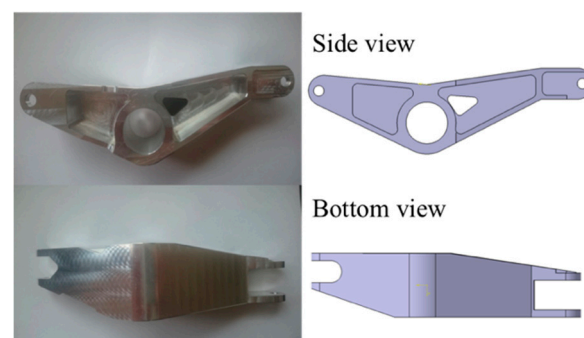

Figure 12. Prototype of optimal design and CAD comparison.

5.4.3. Experimental Validation of Prototype

A final validation after manufacturing of the optimized bell crank was carried out using the same laser vibrometer test. The original part was tested again, as well as the optimized part, to confirm that the optimization of the bell crank has been successful and the same testing conditions had been satisfied. Table 3 shows the natural frequency of the original bell crank compared with the optimized prototype. Overall, the optimized prototype showed an increase in natural frequency of 1.5% compared with the original bell crank. Since the difference was within the 5% limit, the optimization task and the machining can be deemed successful.

Table 3. Summary of laser Vibrometer testing of the original bell crank and optimized prototype.

Location	Original Bell Crank, Frequency (Hz)	Standard Deviation	Optimized Prototype, Frequency (Hz)	Standard Deviation
Location 1	5055.5	1.45	5126.6	0.70
Location 2	5037.5	0.70	5133.7	1.06
Location 3	5056.9	1.48	5119.1	0.58
Location 4	5087.8	1.15	5127.0	1.40
Location 5	5029.6	1.41	5142.4	1.45
Average	5053.3		5129.8	

The final mass of the optimized bell crank design achieved a weight saving of 2.6% (Table 4). Achieving a reduction in mass of the bell crank not only benefits the overall weight of the sidecar, but also reduces the unsprung mass of the suspension system and, therefore, improves the spring/damper unit efficiency [12]. With a careful design interpretation, the optimized design was able to reduce the density of elements within the design domain, while improving the overall stiffness of the bell crank.

Moreover, the optimized design achieved a higher value of natural frequency and lower von Mises stress value under the same static load conditions compared with the original part. The resulting topologically optimized bell crank was mounted in the LCF sidecar as shown in Figure 13.

Table 4. Comparison of original bell crank and optimized prototype.

Parameters	Original Part	Prototype	% of Change
Natural Frequency (Hz)	5053.3	5129.8	+1.5
Max von Mises (MPa)	239.3	199.8	−16.5
Stiffness (k) (MPa)	452.09	455	+0.6
Mass (kg)	0.416	0.405	−2.6
Max strain (-)	3.04×10^{-3}	2.91×10^{-3}	−4.3
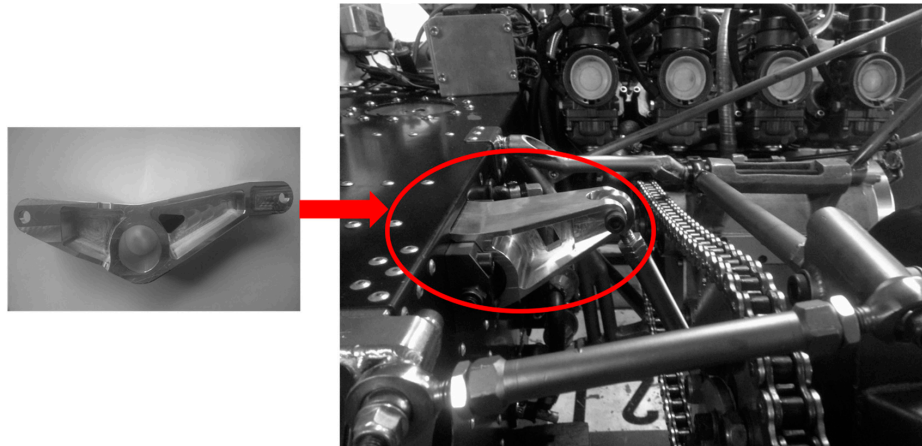
Figure 13. Optimized bell crank in the LCF sidecar.

The modern LCR F1 Sidecar weight is approximately 225 kg, including the engine weight (approximately 50 to 55 kg for current engine specifications). Considering an approximation of 30% to 40% for the sidecar's components (e.g., brake bell, steering, wheel hub and spindle, brake rotor etc.) and further work using the currently proposed methodology that incorporated the topology optimization approach, it was deemed possible that a 5 to 10 kg drop in net weight could be achieved. The methodology described in this paper can be used in mechanical, automotive and aerospace industries for weight reduction design optimization.

In producing a lightweight product, the present study also contributed to enhancing knowledge of how reverse engineering and non-destructive testing methods can be used effectively for structural topology optimization to solve complex designs without compromising performance and integrity.

The emerging of additive manufacturing, especially the 3D printing of metallic materials, will enable the possibilities to further optimize and manufacture bell crank with lattice structures [34], and hence, further work could be carried out for topological optimization of complex design, such as the bell crank and other mechanical components, as miniature lattice structures, which leads to even higher weight reduction.

6. Conclusions

In this paper, a design optimization methodology is described that incorporated: (1) a non-destructive measuring technique using a laser vibrometer; (2) a reverse engineering technique for 3D model construction; and (3) a structural topology optimization. The design optimization methodology was applied to a sidecar suspension bell crank to minimize its structural weight and then subjected to constraints including volume, strain energy and von Mises stress.

A 3D bell crank model was created using a reverse engineering technique and the corresponding FE bell crank model was validated using laser vibrometer test results. The difference between the experimental and FE results of the natural frequency at the fourth mode was less than 5%, which was deemed to be valid for further analysis.

At the beginning of the optimization process, the design domain for material removal was selected. Using the topology optimization approach, the geometry designs produced by the optimization algorithm were transformed into CAD models for the smoothing of the geometry to eliminate holes, irregular shapes and complex edges before fabricating the prototype for further testing. The results obtained from the design optimization methodology demonstrated its applicability and capability to produce an optimized bell crank, which increased its overall stiffness and natural frequency, while reducing its weight by 3%, maximum principal strain by 4.3% and maximum von Mises stress by 16.5%. This study demonstrated how reverse engineering and non-destructive testing methods can be used effectively for structural topology optimization to produce a suitable lightweight product. This is significant contribution to finding solution to complex designs without compromising structural performance and integrity.

Further work using the current methodology could be implemented in other sidecar components (e.g., brake bell, steering, wheel hub and spindle, brake rotor etc.), and additive manufacturing using 3D printing of lattice structures could achieve further net weight reduction.

References

1. Tony, A.; Marcel, E. Bell crank. In *A Dictionary of Mechanical Engineering*; Oxford University Press: Oxford, UK, 2013. [CrossRef]
2. Tsavdaridis, K.D.; Efthymiou, E.; Adugu, A.; Hughes, J.A.; Grekavicius, L. Application of structural topology optimisation in aluminium cross-sectional design. *Thin-Walled Struct.* **2019**, *139*, 372–388. [CrossRef]
3. Aulig, N.; Nutwell, E.; Menzel, S.; Detwiler, D. Preference-based topology optimization for vehicle concept design with concurrent static and crash load cases. *Struct. Multidisc. Optim.* **2018**, *57*, 251–266. [CrossRef]
4. Choudhury, P.; Suresh, N.; Panda, P. Shape Optimization Of A Suspension Bellcrank Using 3d Finite Element Methods. *Int. J. Eng. Res. Appl.* **2015**, *5*, 31–36.
5. Jaafer, A.A.; Al-Bazoon, M.; Dawood, A.O. Structural Topology Design Optimization Using the Binary Bat Algorithm. *Appl. Sci.* **2020**, *10*, 1481. [CrossRef]
6. Fornace, L.V. Weight Reduction Techniques Applied to Formula SAE Vehicle Design: An Investigation in Topology Optimization. Master's Thesis, University of California, San Diego, CA, USA, 2006.
7. Kim, B.-S.; Park, K. Kinematic Motion Analysis and Structural Analysis of Bellcrank Structures Using FEM. *JSAE* **2013**, *6*, 49–55. [CrossRef]
8. Lim, O.; Lee, J. Structural topology optimization for the natural frequency of a designated mode. *KSME Int. J.* **2000**, *14*, 306–313. [CrossRef]
9. Leader, M.K.; Chin, T.W.; Kennedy, G.J. High-Resolution Topology Optimization with Stress and Natural Frequency Constraints. *AIAA J.* **2019**, *57*, 3562–3578. [CrossRef]
10. Thompson, L.; Soni, P.; Raju, S.; Law, E. *The Effects of Chassis Flexibility on Roll Stiffness of a Winston Cup Race Car*; SAE Technical Paper 983051; Society of Automotive Engineers, Inc.: Warrendale, PA, USA, 1998.
11. Bonisoli, E.; Lisitano, D.; Dimauro, L.; Peroni, L. A Proposal of Dynamic Behaviour Design Based on Mode Shape Tracing: Numerical Application to a Motorbike Frame. In *Dynamic Substructures*; Linderholt, A., Allen, M., Mayes, R., Rixen, D., Eds.; Springer: Cham, Switzerland, 2020; Volume 4, pp. 149–158. [CrossRef]
12. Bolles, B. *Advanced Race Car Chassis Technology*; The Penguin Group (USA) Inc.: New York, NY, USA, 2010.
13. Guyan, R.J. Reduction of stiffness and mass matrices. *AIAA J.* **1965**, *3*, 380. [CrossRef]
14. Fard, M.; Yao, J.; Taube, R.; Davy, J.L. The Concept modeling method: An approach to optimize the structural dynamics of a vehicle body. *Proc. Inst. Mech. Eng. Part D J. Automob. Eng.* **2020**, *234*, 2923–2932. [CrossRef]

15. Donders, S.; Takahashi, Y.; Hadjit, R.; Van Langenhove, T.; Brughmans, M.; Van Genechten, B.; Desmet, W. A reduced beam and joint concept modeling approach to optimize global vehicle body dynamics. *Finite Elem. Anal. Des.* **2009**, *45*, 439–455. [CrossRef]

16. Niu, F.; Xu, S.; Cheng, G. A general formulation of structural topology optimization for maximizing structural stiffness. *Struct. Multidisc. Optim.* **2011**, *43*, 561–572. [CrossRef]

17. Asadpoure, A.; Valdevit, L. Topology optimization of lightweight periodic lattices under simultaneous compressive and shear stiffness constraints. *Int. J. Solids Struct.* **2015**, *60–61*, 1–16. [CrossRef]

18. Saleem, W.; Lu, H.; Yuqing, F. Topology Optimization- Problem Formulation and Pragmatic Outcomes by integration of TOSCA and CAE tools. In Proceedings of the World Congress on Engineering and Computer Science 2008, San Francisco, CA, USA, 22–24 October 2008.

19. Bendsøe, M.P.; Sigmund, O. *Topology Optimization Theory, Methods, and Applications*; Springer: Berlin/Heidelberg, Germany, 2004.

20. Lagaros, N.; Vasileiou, N.; Kazakis, G. A C# code for solving 3D topology optimization problems using SAP2000. *Optim. Eng.* **2018**, *20*, 1–35. [CrossRef]

21. Xia, Q.; Shi, T.; Wang, M.Y. A level set based shape and topology optimization method for maximizing the simple or repeated first eigenvalue of structure vibration. *Struct. Multidisc. Optim.* **2011**, *43*, 473–485. [CrossRef]

22. Spelsberg-Korspeter, G. Eigenvalue optimization against brake squeal: Symmetry, mathematical background and experiments. *J. Sound Vib.* **2012**, *331*, 4259–4268. [CrossRef]

23. Wu, B.; Yang, S.; Li, Z.; Zhong, H.; Chen, X. Computation of frequency responses and their sensitivities for undamped systems. *Eng. Struct.* **2019**, *182*, 416. [CrossRef]

24. Thomas, J.; Sahu, A.K.; Mahapatra, S.S. Simple Optimization Algorithm for Design of a Uniform Column. In *Advances in Applied Mechanical Engineering*; Voruganti, H., Kumar, K., Krishna, P., Jin, X., Eds.; Springer: Gateway East, Singapore, 2020; pp. 351–362. [CrossRef]

25. Trainotti, F.; Berninger, T.F.C.; Rixen, D.J. Using Laser Vibrometry for Precise FRF Measurements in Experimental Substructuring. In *Dynamic Substructures*; Linderholt, A., Allen, M., Mayes, R., Rixen, D., Eds.; Springer: Cham, Switzerland, 2020; Volume 4, pp. 1–11. [CrossRef]

26. *ABAQUS, Version 6.14*; Dassalt Systemés: Providence, RI, USA, 2014.

27. Huuki, J.; Hornborg, M.; Juntunen, J. Influence of Ultrasonic Burnishing Technique on Surface Quality and Change in the Dimensions of Metal Shafts. *J. Eng.* **2014**, *2014*, 8. [CrossRef]

28. Kim, D.Y.; Kang, W.J.; Cho, H.M.; Cheon, S.S. Analytical Evaluation of Al 6082-T6 Weld Zone Using Randomised Mixing Material Model. *Appl. Mech. Mater.* **2013**, *302*, 55. [CrossRef]

29. Manios, S.E.; Lagaros, N.D.; Nassiopoulos, E. Nested Topology Optimization Methodology for Designing Two-Wheel Chassis. *Front. Built Environ.* **2019**, *5*. [CrossRef]

30. Eibach. *Motorsport Catalog*; Eibach Springs, Inc.: Corona, CA, USA, 2014.

31. Prantil, V.C.a.; Papadopoulos, C.; Gessler, P.D. *Lying by Approximation: Truth about Finite Element Analysis*; Morgan & Claypool Life Sciences: San Rafael, CA, USA, 2013.

32. Liu, K.; Tovar, A. An efficient 3D topology optimization code written in Matlab. *Struct. Multidisc. Optim.* **2014**, *50*, 1175–1196. [CrossRef]

33. Zuo, K.-T.; Chen, L.-P.; Zhang, Y.-Q.; Yang, J. Manufacturing- and machining-based topology optimization. *Int. J. Adv. Manuf. Technol.* **2006**, *27*, 531–536. [CrossRef]

34. Terriault, P.; Brailovski, V. Modeling and simulation of large, conformal, porosity-graded and lightweight lattice structures made by additive manufacturing. *Finite Elem. Anal. Des.* **2018**, *138*, 1–11. [CrossRef]